The Ocular Surface 17 (2019) 777–786

Contents lists available at ScienceDirect

The Ocular Surface

journal homepage: www.elsevier.com/locate/jtos

Original Research

Hyperlipidemia induces meibomian gland dysfunction

Jinghua Bu[a,1], Yang Wu[a,1], Xiaoxin Cai[a], Nan Jiang[a], M. Vimalin Jeyalatha[a], Jingwen Yu[a], Xin He[a], Hui He[a], Yuli Guo[a], Mingjie Zhang[a], Andrew J. Quantock[b], Zuguo Liu[a], Wei Li[a,*]

[a] Department of Ophthalmology, Xiang'an Hospital of Xiamen University; Fujian Provincial Key Laboratory of Ophthalmology and Visual Science; Eye Institute of Xiamen University; School of Medicine, Xiamen University, China
[b] School of Optometry and Vision Sciences, Cardiff University, Cardiff, UK

ARTICLE INFO

Keywords:
Apolipoprotein E
Meibomian gland dysfunction
Hyperlipidemia
Inflammation
PPAR-γ

ABSTRACT

Purpose: To investigate the pathological changes of the meibomian gland (MG) and ocular surface in Apolipoprotein E knockout ($ApoE^{-/-}$) mice and to investigate the association of meibomian gland dysfunction (MGD) with hyperlipidemia.

Methods: Total plasma cholesterol was measured in different ages of $ApoE^{-/-}$ and wild type (WT) mice, whilst the ocular surfaces were observed by slit-lamp biomicroscopy. MG sections were subjected to H&E staining, Oil Red O staining, TUNEL assay and immunostaining. Quantitate RT-PCR and Western blot analyses were performed to detect the relative gene expression in MGs. The 5-month-old $ApoE^{-/-}$ mice were administered with rosiglitazone or GW9662 + rosiglitazone via oral gavage for 2 months to determine their effect on MG pathological change.

Results: We found eyelid abnormality, MG dropout, abnormal MG acinar morphology, dilated MG duct and plugging of the MG orifice in $ApoE^{-/-}$ mice. MG acini in $ApoE^{-/-}$ mice showed exaggerated lipid accumulation. Abnormal keratinization increased in MG duct, accompanied with decreased proliferation and increased apoptosis in $ApoE^{-/-}$ mice. Inflammatory cells infiltrated into the surrounding microenvironment of MG acini, and the NF-κB signaling pathway was activated in MG acinar cells. Oxidative stress was evident in MG acinar cells of $ApoE^{-/-}$ mice. Further investigation showed downregulation of PPAR-γ in MG acinar cells of $ApoE^{-/-}$ mice. PPAR-γ agonist rosiglitazone treatment reduced the morbidity of eyelid, as well as corneal pathological changes and MG inflammation in $ApoE^{-/-}$ mice.

Conclusion: MGD and hyperlipidemia are closely associated in $ApoE^{-/-}$ mice, which represent a new model to study the pathophysiology of MGD related to dyslipidemia.

1. Introduction

Meibomian glands (MGs), a type of modified, holocrine sebaceous glands of the eyelid margin, are arranged vertically in the upper and lower tarsal plates [1]. MGs maintain ocular surface homeostasis by secreting specialized lipids to the tear film, which functions to avert tear evaporation, smoothen the ocular surface, and form a barrier to protect the eye from microbial agents and organic matter [2–6]. Meibomian gland dysfunction (MGD) is defined as a chronic, diffuse abnormality of the MGs, commonly characterized by terminal duct obstruction and/or qualitative/quantitative changes in the glandular secretion [7]. MGD may result in alteration of the tear film stability, symptoms of eye irritation, clinically apparent inflammation, and ocular surface disease [2,8]. MGD is the most common cause of evaporative dry eye [9], and results in significant negative effects on life quality of the dry eye sufferers [10,11].

Apolipoprotein E (ApoE) is a component of plasma lipoproteins and serves as a ligand for cell-surface lipoprotein receptors such as low density lipoprotein (LDL)-receptor (LDLR), LDLR related proteins, very low-density lipoprotein (VLDL), and high-density lipoprotein (HDL) [12]. It is synthesized in the liver and macrophages, and plays an important role in mediating cholesterol metabolism in an isoform-dependent manner [13,14]. Apolipoprotein E knockout ($ApoE^{-/-}$) mice are characterized by marked increase in total plasma cholesterol levels of more than 500 mg/dL, and develop microvasculature lesions [15]. They also demonstrate decreased clearance of remnant lipoproteins that

* Corresponding author. Eye Institute of Xiamen University, Xiang'an Hospital of Xiamen University, School of Medicine, Xiamen University, 4th Floor, 4221-122, South Xiang'an Rd, Xiamen, Fujian, 361102, China.
E-mail address: wei1018@xmu.edu.cn (W. Li).
[1] These authors contributed equally to this work thus should be considered as co-first authors.

https://doi.org/10.1016/j.jtos.2019.06.002
Received 19 April 2019; Received in revised form 28 May 2019; Accepted 10 June 2019

leads to hypercholesterolemia and hypertriglyceridemia [16]. The lesions increase with age and progress to atherosclerotic lesion [17]. Thus, *ApoE*$^{-/-}$ mice are the most widely used murine model to study the mechanisms of hyperlipidemia and atherosclerosis [18,19].

In recent years, several clinical studies reported that patients with moderate-to-severe MGD had abnormal serum cholesterol levels [20,21], and that the severity of the MGD increased with high serum triglyceride and low-density lipoprotein levels [22]. These findings suggest that MGD may be related to abnormal lipid metabolism. However, whether or not the MGD has a direct relationship with dyslipidemia remains elusive. In this study, we investigated the pathological changes of the MG and ocular surface in *ApoE*$^{-/-}$ mice and illustrate a clear association of MGD with hyperlipidemia.

2. Materials and methods

2.1. Materials

Rabbit anti-Ki67 (ab16667), anti-P63 (ab124762), anti-Cytokeratin 10 (ab76318), anti-TNF-α (ab66579), anti-NADPH oxidase 4 (NOX-4, ab133303), anti-4 Hydroxynonenal (4-HNE, ab46545), anti-PPAR-γ (ab45036) antibodies, and mouse anti-3-Nitrotyrosine antibody (3-NT ab61392) were from Abcam (Cambridge, UK). Rabbit anti-AC-caspase-8 (sc-7890), rat anti-CD45 (sc-52491) antibodies, Rosiglitazone (sc-202795) and GW9662 (sc-202641) were from Santa Cruz Biotechnology (Dallas, TX, USA). Rabbit anti-IL-6 (Cat#12912S), anti-NF-κB p65 (Cat#8242) and anti-phospho-NF-κB p65 (Cat#3033) antibodies were from Cell Signaling Technology (Danvers, MA, USA). Anti-FABP5 (PA5-47143), Alexa Fluor 594-conjugated IgG (A11058) and Alexa Fluor 488-conjugated IgG (A11055, A21206) were from Invitrogen (Eugene, OR, USA). Horseradish peroxidase (HRP)-conjugated anti-β-actin antibody (a5316) was from Sigma-Aldrich (St. Louis, MO, USA). 40,6-diamidino-2-phenylindole (DAPI; H-1200) and mounting medium (H-5000) were from Vector (Burlingame, CA, USA).

2.2. Animals

Male *ApoE*$^{-/-}$ mice aged 3, 5, and 7 months and age and sex matched wild type (WT) mice were used in this study. The *ApoE*$^{-/-}$ mice were from Beijing Vital River Laboratory Animal Technology Co., Ltd (Beijing, China), and the wild-type C57BL/6 mice were purchased from Shanghai SLAC Laboratory Animal Center (Shanghai, China). All studies were performed in accordance with the Association for Research in Vision and Ophthalmology (ARVO) Statement for the Use of Animals in Ophthalmic and Vision Research, and with the approval of the Animal Ethical Committee of Xiamen University. Animals were given free access to standard rodent chow and water and kept in standard pathogen-free environment at 25 °C ± 1 °C, relative humidity 60% ± 10%, and alternating 12 h light-dark cycles (from 8:00 a.m. to 8:00 p.m.).

2.3. Animal examination

All the animals were weighed, after which the eyelid margins and corneas were imaged in a masked fashion under a slit-lamp microscope (Kanghua Science & Technology Co. Ltd., Chongqing, China) by a single ophthalmologist. After that, 1 μL of 1% liquid sodium fluorescein (Jingmingxin Co., Ltd., Tianjin, China) was dropped into the conjunctival sac, and corneal epithelial fluorescein staining was recorded 90 s later under the slit-lamp microscope with a cobalt blue filter. The grade of corneal damage was designated based on previously reported criteria [23]. Corneal neovascularization was also observed and recorded. Five mice in each group were sacrificed and the upper and lower eyelids were excised en bloc, after which the MG structure was clinically photographed with a stereoscopic zoom microscope (Leica M165-FC; Germany).

2.4. Plasma cholesterol measurements

Blood samples (five mice per group) were collected from both WT and *ApoE*$^{-/-}$ mice by cardiac puncture at the time of sacrifice and stored at −80 °C. Serum total cholesterol was measured enzymatically using a commercially available kit (ab65390, Abcam, Cambridge, UK) in accordance with the manufacturer's instructions.

2.5. Histology

Eyelid tissues were collected from WT and *ApoE*$^{-/-}$ mice and embedded in optimal cutting temperature (OCT) compound or paraffin, cut into sagittal sections (5 μm thick, two sections per slide, three slides per animal, three animals per group), and then stored at −80 °C (frozen sections) or room temperature (paraffin sections). Immunohistochemical staining and TUNEL assay were performed on the paraffin sections, and immunofluorescence staining, Oil Red O, Hematoxylin and Eosin staining were performed on frozen sections.

2.6. Oil Red O staining

Frozen eyelid sections were fixed in 4% paraformaldehyde for 10 min, washed in PBS for 5 min, and stained for 10 min in freshly prepared Oil Red O solution. After rinsing with PBS for 5 min, the sections were counterstained with hematoxylin and mounted in 90% glycerol.

2.7. TUNEL assay

Cell apoptosis detection was performed using the DeadEnd™ Fluorometric TUNEL System (Promega, G3250). MG sections were rehydrated and incubated with Proteinase K Tris/HCL, pH = 7.4 (10 mM) for 30 min at 37 °C. The MG sections were washed three times with PBS for 5 min each. Then, 50 μL of TUNEL reaction mixture was added and the sections placed in the dark for 1 h at 37 °C. The specimens were rinsed three times with PBS for 5 min each, counterstained with DAPI, mounted, and photographed with a microscope (DM2500; Leica Microsystems, Wetzlar, Germany).

2.8. Immunofluorescence staining

For immunofluorescence staining, sections were fixed in cold acetone (−20 °C) for 10 min followed by washing three times using PBS for 5 min each. Sections were incubated with 0.2% Triton X-100 for 20 min and again washed three times each with PBS for 5 min. Tissue sections were then blocked with 2% BSA in PBS for 60 min at room temperature and incubated with Ki67 (1:300), p63 (1:200), Cytokeratin 10 (1:200), FABP5 (1:50), AC-caspase-8 (1:50), IL-6 (1:200), TNF-α (1:200), NF-κB p65 (1:200), phospho-NF-κB p65 (1:200), PPAR-γ (1:250) antibodies for 16 h at 4 °C. Negative controls were performed by incubating a section with PBS without the primary antibody. The slides were then washed three times with PBS for 10 min per wash and incubated with Alexa Fluor 594-conjugated IgG (1:300) or Alexa Fluor 488-conjugated IgG (1:300) for 60 min at 37 °C, followed by counterstaining with DAPI. Sections were then evaluated and imaged with a microscope (DM2500; Leica Microsystems, Wetzlar, Germany). The mean intensity of staining in some sections was measured by image analysis software (NIS Elements version 4.1, Nikon, Melville, NY, USA).

2.9. Immunohistochemical staining

Paraffin sections were rehydrated and blocked with 3% hydrogen peroxide for 10 min, followed by washing three times with PBS for 5 min each. Sections were subsequently treated with 0.2% Triton X-100 for 20 min. After washing three times each with PBS for 5 min, they were incubated with 2% BSA for 60 min, followed by incubation with

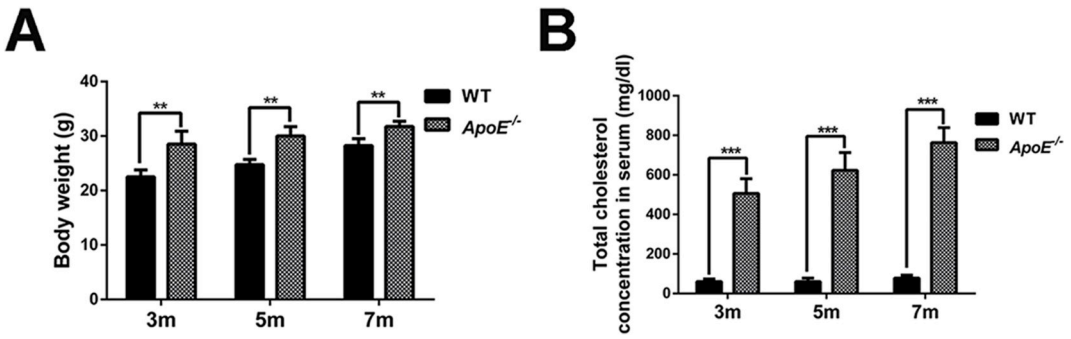

Fig. 1. Systemic characteristics of *ApoE*$^{-/-}$ mice. Body weight increased in *ApoE*$^{-/-}$ mice compared with WT mice (**A**). Total cholesterol concentrations in the serum (**B**). Data are shown as mean ± SD. $^{**}p < 0.01$, $^{***}p < 0.001$.

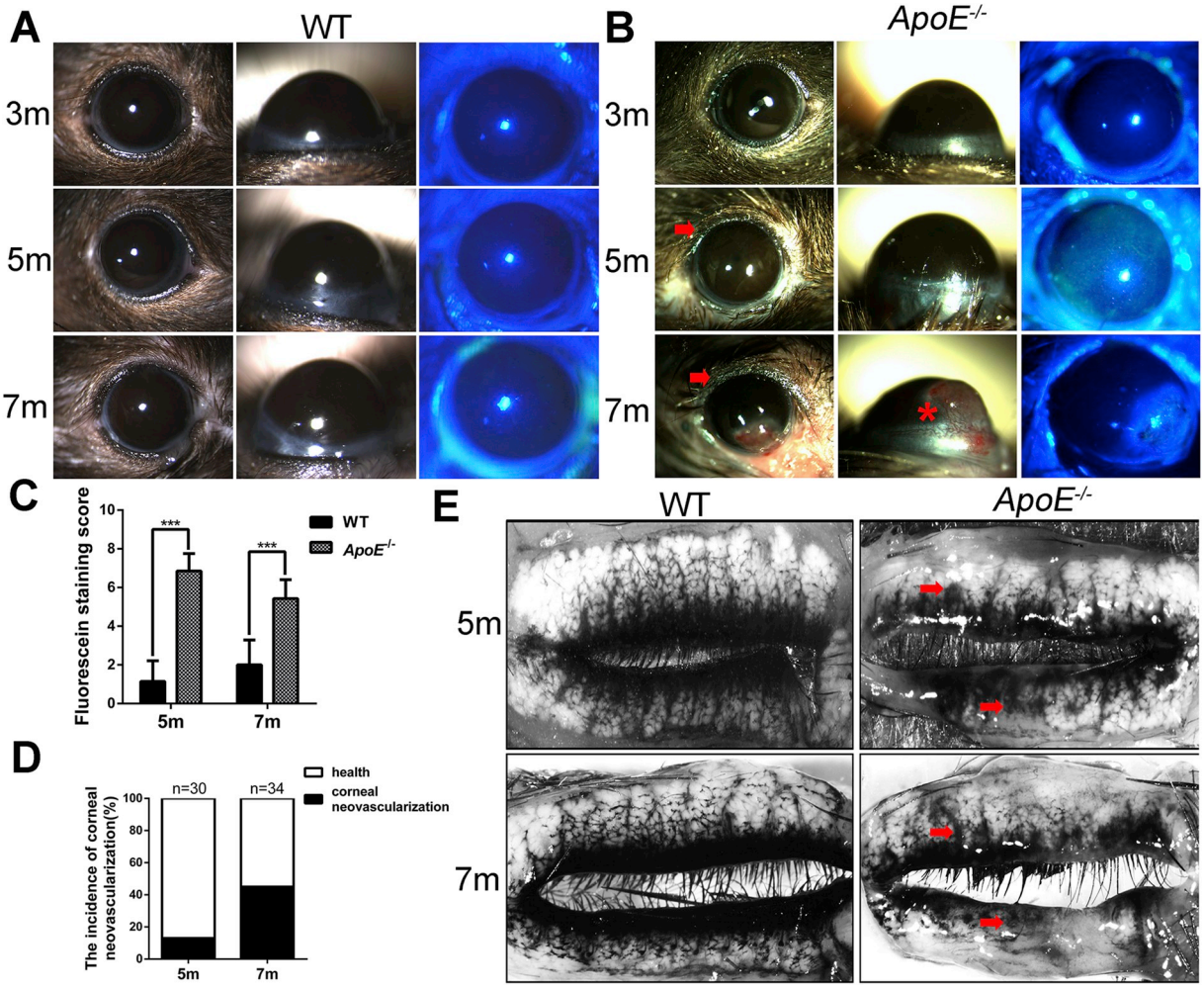

Fig. 2. *ApoE*$^{-/-}$ mice exhibits clinical evidence of MGD. Representative slit-lamp images showing the ocular surface of WT mice (**A**) and hypertrophic eyelid margins (arrow heads) and corneal neovascularization (7 months, asterisk) in *ApoE*$^{-/-}$ mice (**B**). The fluorescein staining score (**C**) and corneal neovascularization incidence rate (**D**) increased in *ApoE*$^{-/-}$ mice. MG dropout (arrow heads) and morphological changes are seen in *ApoE*$^{-/-}$ mice in both upper and lower MGs (E). Data are shown as mean ± SD. $^{***}p < 0.001$.

CD45 (1:150), NOX-4 (1:250), 3-NT (1:200), and 4-HNE (1:200) antibodies at 4 °C for 16 h. The next day, after rinsing three times with PBS for 10 min each, the sections were further incubated with biotinylated anti-rabbit IgG (1:50), anti-rat IgG (1:50) or anti-mouse IgG (1:50) for 60 min, followed by Vectastain Elite ABC reagent for 30 min. The reaction product was then developed with diaminobenzidine (DAB) for 1 min, mounted with mounting medium, and examined under a light microscope (Eclipse 50i; Nikon, Tokyo, Japan). Positively stained cells were counted in the MGs using NIS Elements image analysis software (NIS Elements version 4.1; Nikon, Melville, NY, USA).

2.10. RNA extraction and qRT-PCR

MGs were isolated under a dissecting microscope by the removal of skin, subcutaneous tissue, muscle, and palpebral conjunctiva. RNA sample parameters and concentrations were detected by a Du 800 Nucleic Acid/protein Analyzer (Beckman coulter, US). Five samples were used in each group, and one sample consisted of pooled MGs of

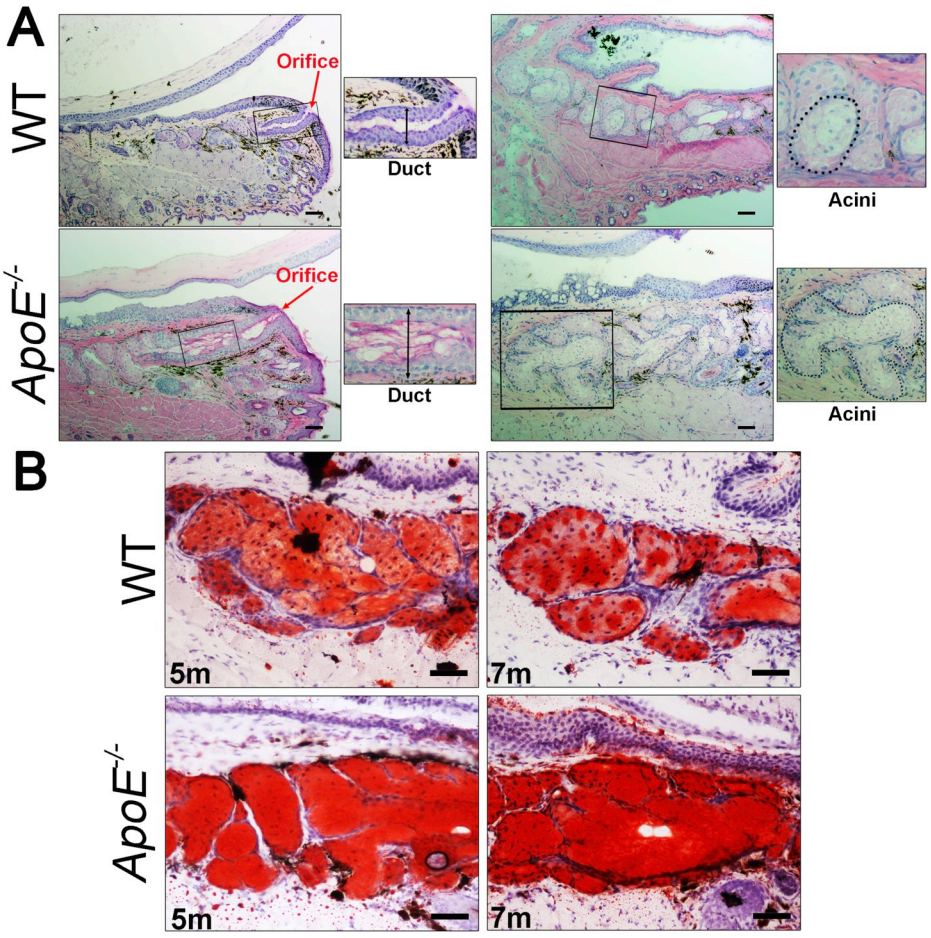

Fig. 3. *ApoE*$^{-/-}$ mice exhibit histological evidence of MGD. Representative H&E staining of eyelids from 7-month-old WT and *ApoE*$^{-/-}$ mice. Red arrow heads indicating the obstructed MG orifice in *ApoE*$^{-/-}$ mice and unobstructed orifice in WT mice. Black double-headed arrows showing MG duct size, indicating that the MG duct in *ApoE*$^{-/-}$ mice is significantly dilated. Representative images of acini showing alterations in acinar morphology in *ApoE*$^{-/-}$ mice (**A**). ORO staining showing condensed lipid droplets in the MGs of *ApoE*$^{-/-}$ mice (**B**). Scale bars: 50 μm.

both eyes of the same mice. The equal amount of RNA was reverse transcribed to cDNA using a reverse transcription kit (RR047A; TaKaRa, Shiga, Japan). Quantitative Real-Time PCR (qRT-PCR) was performed with a StepOneTM Real-Time PCR detection system (Applied Biosystems, Alameda, CA, USA) using a SYBR Premix Ex TaqKit (RR420A; TaKaRa, Shiga, Japan), and the specific primer sequences are available upon request. The thermal profile used was as follows: 95 °C for 10 min, followed by denaturation at 95 °C for 10 s and annealing and extension at 60 °C for 30 s for 40 cycles. The results of qRT-PCR were analyzed by the comparative CT method and normalized with β-actin as an endogenous reference, and calibrated against the normal control group.

2.11. Western blot analysis

Isolated MGs were extracted in a cold lysis buffer composed of protease and phosphatase inhibitor. Protein concentration was measured by BAC protein assay kit (cat#23225; ThermoFisher Scientific, MA, USA). Five samples were used in each group, and each sample consisted of pooled MGs of both eyes of the same mice. Equal amounts of protein extracts (20 μg) were subjected to electrophoresis on 10% Tricine gels and then electronically transferred to PVDF membranes. After blocking in 5% BSA for 1 h, the membranes were incubated overnight at 4 °C with primary antibodies for NF-κB p65 (1:1000), phospho-NF-κB p65 (1:1000), NOX-4 (1:1000), 3-NT (1:1000), 4-HNE (1:1000), PPAR-γ (1:1000) and secondary antibodies (HRP-conjugated goat anti-mouse IgG and HRP-conjugated goat anti-rabbit IgG) were used. HRP-conjugated mouse anti–β-actin was used for protein quantification. The results were detected by enhanced chemiluminescence reagent (ECL-500; ECL, Lulong Inc, Xiamen, China) and recorded by the transilluminator (ChemiDoc XRS System; Bio-Rad, Philadelphia, PA, USA).

2.12. Statistical analysis

Data were processed using GraphPad Prism 6.0 software (GraphPad Software Inc, San Diego, CA, USA). Statistical analysis was performed using the Mann-Whitney test to compare the differences in body weight, relative mRNA rate, cholesterol concentration, corneal fluorescein staining scores, Ki67, P63 and CD45 positive cell counting, intensity of AC-caspase-8 immunofluorescent staining, apoptotic cell counting. A one-way ANOVA was conducted to analyze differences in corneal fluorescein staining scores and CD45 positive cell counting in drug treatment experiments. A value of $p < 0.05$ was considered statistically significant.

3. Results

3.1. Eyelid and ocular surface manifestations of *ApoE*$^{-/-}$ mice

Mice were followed up for 7 months during which time the body mass of *ApoE*$^{-/-}$ mice had become significantly higher than that of WT mice from 3 to 7 months (Fig. 1A). There was also a significant increase of total cholesterol in the serum of *ApoE*$^{-/-}$ mice compared to the age-matched WT mice (Fig. 1B), similar to previous reports [24], suggesting that *ApoE*$^{-/-}$ mice are indeed an appropriate model of hyperlipidemia.

Slit lamp images showed no obvious changes in either the eyelids or the corneas of WT mice from 3 months to 7 months (Fig. 2A). However, there was a notable amount of punctate corneal staining in 5-month-old *ApoE*$^{-/-}$ mice, which was accompanied by corneal neovascularization

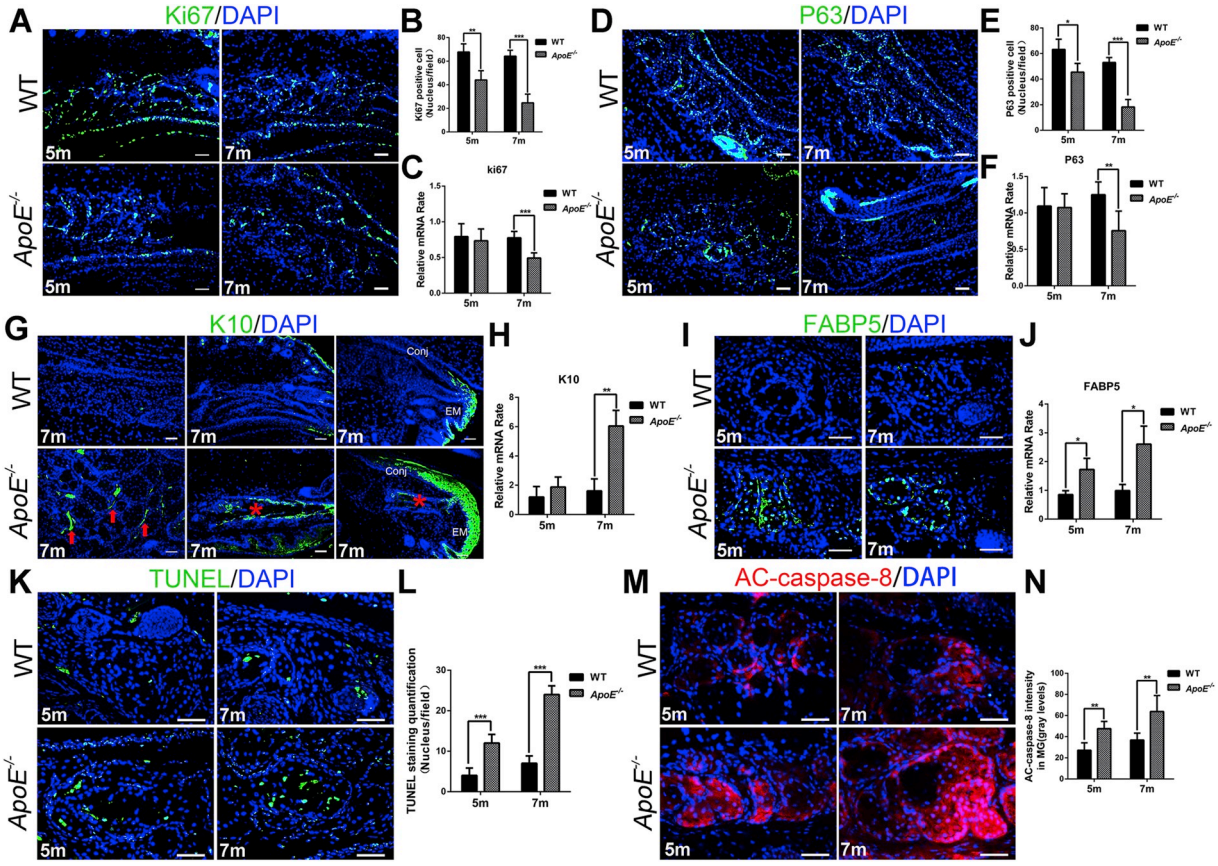

Fig. 4. Reduced proliferation, hyperkeratinization and increased apoptosis in MG of *ApoE*$^{-/-}$ mice. Ki67 immunofluorescence staining (**A**), positive cell counts (**B**), and gene expression (**C**) decreased in *ApoE*$^{-/-}$ mice. P63 immunofluorescence staining (**D**), positive cell counts (**E**), and gene expression (**F**) also decreased in *ApoE*$^{-/-}$ mice. K10 positive cells increased in MG acini (arrow heads), duct (asterisk) and the eyelid margin of 7-month-old *ApoE*$^{-/-}$ mice (**G**). K10 gene expression is upregulated in *ApoE*$^{-/-}$ mice (**H**). Immunofluorescent staining (**I**) and mRNA expression (**J**) of FABP5 showing significant up-regulation in MGs of *ApoE*$^{-/-}$ mice compared with those of WT mice. Increased TUNEL assay staining (**K**) and cell counts (**L**) reveal increased apoptosis of acinar cells in MGs of *ApoE*$^{-/-}$ mice compared with those of WT mice. AC-caspase-8 immunofluorescent staining (**M**) and intensity analysis (**N**) indicates higher AC-caspase-8 expression in MGs of *ApoE*$^{-/-}$ mice compared with those of WT mice. Data are shown as mean ± SD. $^{*}p < 0.05$, $^{**}p < 0.01$, $^{***}p < 0.001$. Scale bars: 50 μm. Conj, conjunctiva; EM, eyelid margin.

at 7-months (Fig. 2B). The eyelids from *ApoE*$^{-/-}$ mice were also noticeably hypertrophic compared with the eyelids of WT mice at 5 and 7 months (Fig. 2B). Corneal fluorescein staining increased remarkably in *ApoE*$^{-/-}$ mice compared to the WT mice at 5 and 7 months (Fig. 2C). The incidence of corneal neovascularization also dramatically increased in 7-month-old *ApoE*$^{-/-}$ mice (Fig. 2D). MG dropout and plugging of the MG orifice are key clinical signs of MGD [25,26]. Obvious MG dropout with disordered acini and ducts in *ApoE*$^{-/-}$ mice was seen in both the upper and lower glands in contrast to the dense and organized MGs in WT mice (Fig. 2E).

H&E staining revealed plugging of the MG orifice, dilation of duct and heteromorphic acinar morphology (Fig. 3A). In addition, MGs of *ApoE*$^{-/-}$ mice showed more condensed ORO staining, especially at the 7 month timepoint (Fig. 3B). Taken together, it is evident that MG obstruction occurs in *ApoE*$^{-/-}$ mice, accompanied with MG dropout and alterations in MG morphology and function.

3.2. Pathological change of MG cells in ApoE$^{-/-}$ mice

We further investigated the proliferation, differentiation and apoptosis of MG cells in 5 and 7 month old mice. Ki67 positive cells were decreased in the acini of MGs from 5 to 7 month old *ApoE*$^{-/-}$ mice compared to the age matched WT mice (Fig. 4A and B). This was further confirmed by Ki67 gene expression (Fig. 3C). The P63 gene, which is strongly expressed in epithelial cells with high clonogenic and proliferative capacity [27], was apparently decreased in acini in 5 and 7 months old *ApoE*$^{-/-}$ mice (Fig. 4D and E), as seen by immune-localization and confirmed by qRT-PCR (Fig. 4F).

Hyper-keratinization is a major pathological change of obstructive MGD that can result in degenerative gland dilatation and atrophy [28–30]. K10 is the marker for terminally keratinized epithelium [31]. FABP5 is another keratinization marker, which could induce increased expression of K10 and involucrin in human keratinocytes [32]. FABP5 is also highly expressed in spinous layers along with upregulation of K10 in psoriatic skin [33]. Immunofluorescence staining revealed positive K10 cells in MG acini and duct in 7-month-old *ApoE*$^{-/-}$ mice, but only a scant number of positive cells in the MG duct of WT mice (Fig. 4G). In addition, the 7-month-old *ApoE*$^{-/-}$ mice showed thickening and hyperkeratosis of the eyelid margin with the K10 positive cells extended to the palpebral conjunctiva (Fig. 4G, EM). No significant difference was noticed in 5-month-old *ApoE*$^{-/-}$ and WT mice (data not shown). qRT-PCR confirmed upregulated K10 gene expression in MG tissue of 7-month-old *ApoE*$^{-/-}$ mice (Fig. 4H). FABP5 was also highly expressed in 5 and 7 month old *ApoE*$^{-/-}$ mice (Fig. 4I), as was confirmed by qRT-PCR (Fig. 4J). These results indicated that the MGs from *ApoE*$^{-/-}$ mice were excessively keratinized.

Quantification of TUNEL positive cells revealed that apoptosis was promoted in MGs of *ApoE*$^{-/-}$ mice at both 5 and 7 months (Fig. 4K and L). The immunofluorescence staining found up-regulated AC-caspase-8 expression in *ApoE*$^{-/-}$ mice compared with that seen in WT mice (Figure 4M, N), further pointing to apoptosis in the MG in the mutant mice.

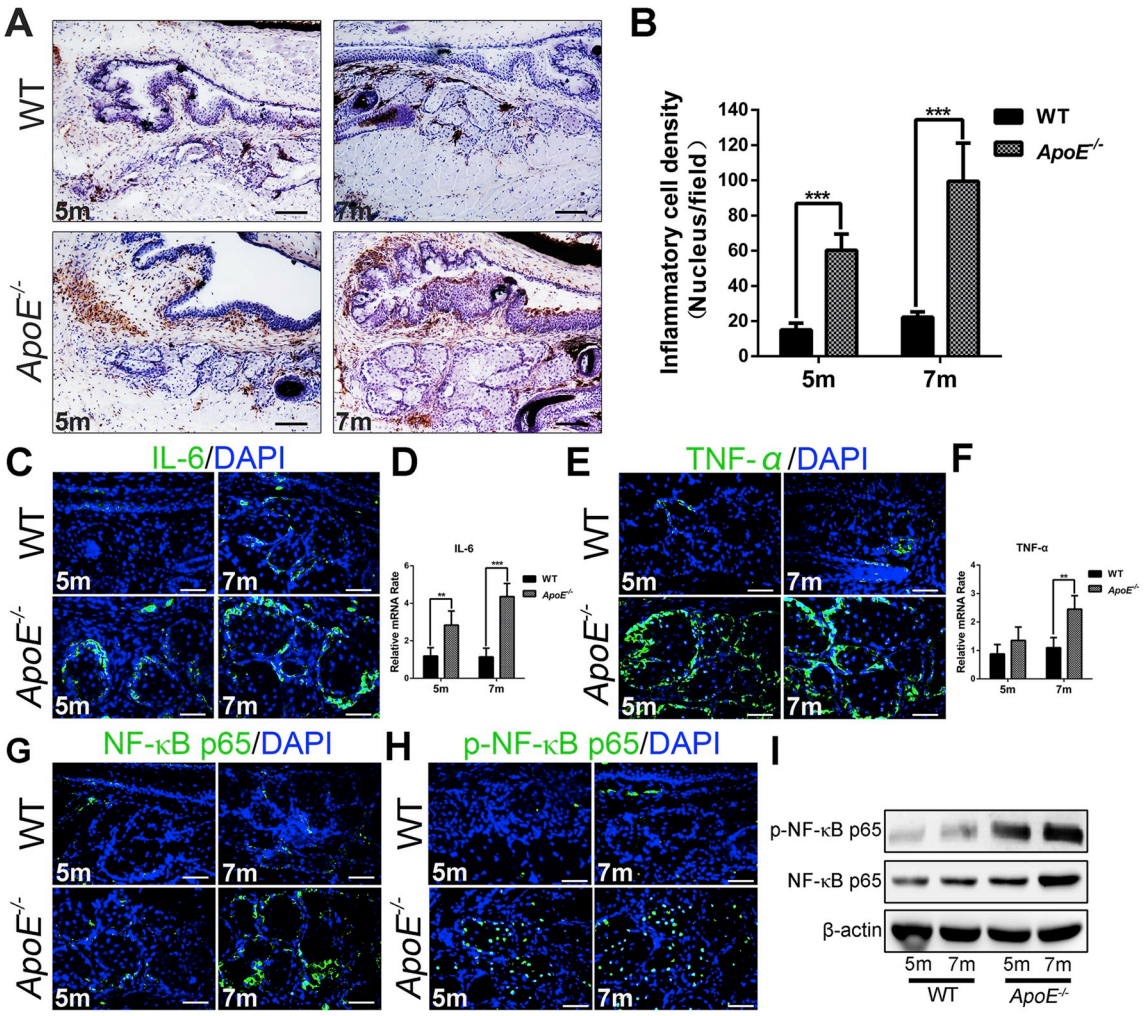

Fig. 5. Inflammation in MG of *ApoE*$^{-/-}$ mice. Immunohistochemistry shows CD45 positive cell infiltration surrounding the acini of MGs (**A**), and a CD45 positive cell density that is dramatically increased in the *ApoE*$^{-/-}$ mice (**B**). Immunofluorescence staining and mRNA levels of IL-6 (**C, D**) and TNF-α (**E, F**) disclose significant upregulation in MGs of *ApoE*$^{-/-}$ mice compared to those of WT mice. Immunofluorescence of NF-κB p65 (**G**) and p-NF-κB p65 (**H**), and Western blot analysis (**I**) is indicative of an activated NF-κB signaling pathway in MGs of *ApoE*$^{-/-}$ mice. Data are shown as mean ± SD. $^{**}p < 0.01$, $^{***}p < 0.001$. Scale bars: 50 μm.

3.3. Eyelid tissue inflammation in *ApoE*$^{-/-}$ mice

CD45 immunohistochemistry staining showed intense periglandular staining in the MGs of *ApoE*$^{-/-}$ mice (Fig. 5A), with a higher number of positive cells than in WT mice (Fig. 5B). IL-6 and TNF-α expression were significantly increased in the basal acinar and stromal cells of MGs in *ApoE*$^{-/-}$ mice compared to MGs of WT mice (Fig. 5C, D, E, and F). Immunofluorescence staining and Western blot results showed up-regulation of both NF-κB p65 and p-NF-κB p65 in *ApoE*$^{-/-}$ mice (Fig. 5 G, H and I). These results indicated that *ApoE*$^{-/-}$ mice have increased levels of IL-6 and TNF-α, in part, through an enhancement of the NF-κB pathway in MG.

3.4. Oxidative stress in MG of *ApoE*$^{-/-}$ mice

A significant increase of NOX-4 nuclear staining was observed in the acinar epithelial cells of 5 and 7 month old *ApoE*$^{-/-}$ mice compared with WT mice (Fig. 6A). We also observed a marked increase of 3-NT and 4-HNE expression in MGs from *ApoE*$^{-/-}$ mice compared with WT mice at 5 and 7 months (Fig. 6B and C). Western blot results confirmed upregulated protein expression of NOX-4, 3-NT and 4-HNE in MGs of *ApoE*$^{-/-}$ mice (Fig. 6D).

3.5. MG differentiation change in *ApoE*$^{-/-}$ mice

The terminal differentiation of sebocytes inside the MG acinus is maintained by peroxisome proliferator-activated receptor-gamma (PPAR-γ), which is a key factor for all lipid-synthesizing cells [34]. The expression pattern of PPAR-γ gradually redistributes from the cytoplasm in infant and young adult mice to the nucleus in old mice [35]. Cytoplasm to nuclear translocation of PPAR-γ was also observed in aged-related MGD [36].

Immunofluorescence staining showed nuclear and cytoplasmic staining of PPAR-γ in meibocytes of WT mice, whereas in *ApoE*$^{-/-}$ mice the staining pattern was exclusively observed only in the nucleus (Fig. 6E). Western blot results showed that PPAR-γ was significantly decreased in *ApoE*$^{-/-}$ mice compared to WT mice (Fig. 6F and G).

3.6. PPAR-γ agonist treatment prevent MG pathological change in *ApoE*$^{-/-}$ mice

Rosiglitazone (ROSI) is a specific PPAR-γ agonist and GW9662 is a specific PPAR-γ antagonist. To further determine the function of PPAR-γ in MGs, 5 months old *ApoE*$^{-/-}$ mice (n = 30) were randomly divided into a control (CON) group (PBS containing 0.01% DMSO, oral gavage, one time daily, n = 10), a ROSI group (10 mg/kg, oral gavage, one time daily, n = 10) and a GW9662 (3 mg/kg, oral gavage, 60 min before

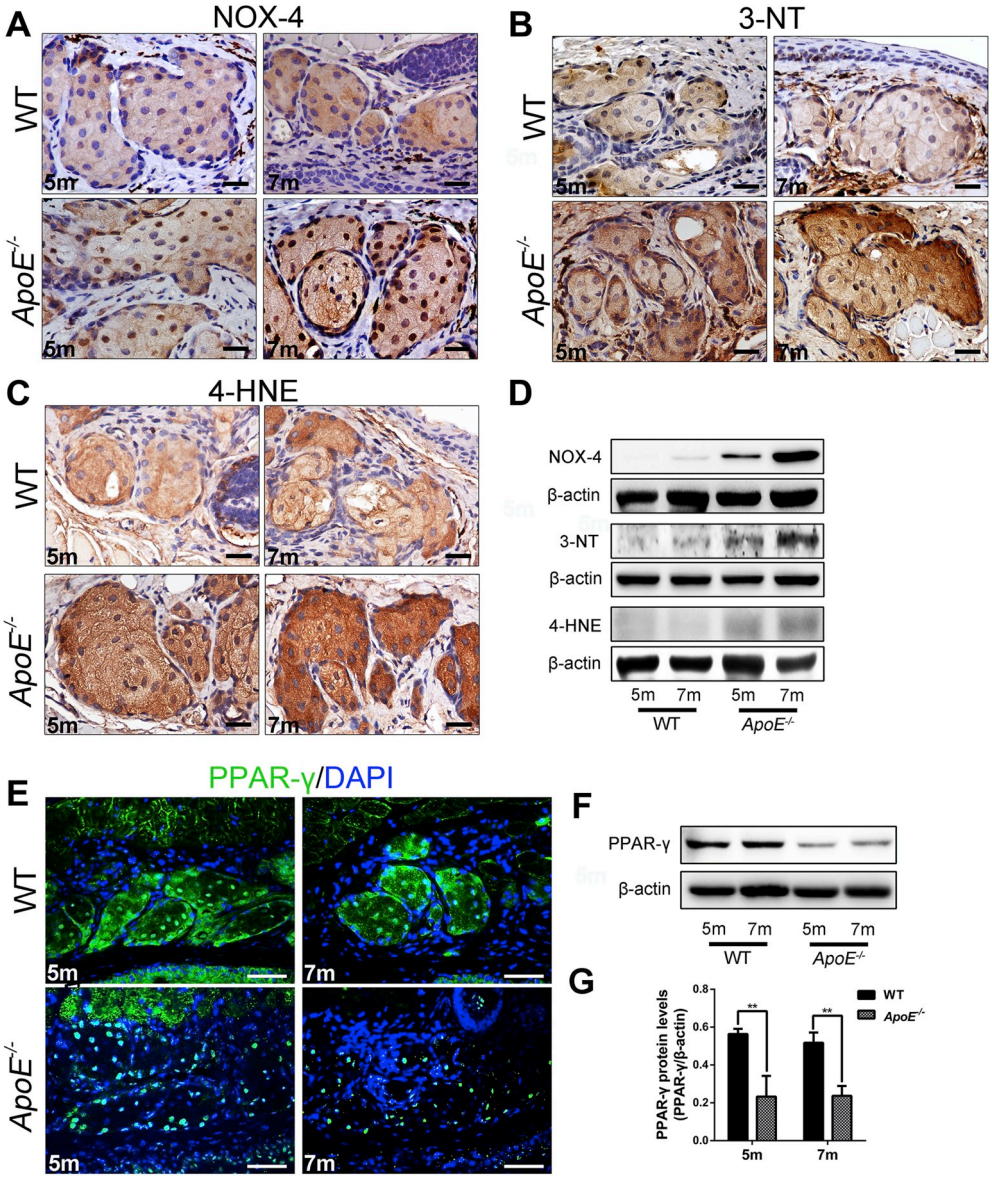

Fig. 6. Activation of oxidative stress and down-regulation of PPAR-γ in *ApoE*$^{-/-}$ mice. Immunohistochemical staining shows a relatively increased expression of oxidative stress markers NOX-4 (**A**), 3-NT (**B**) and 4-HNE (**C**) in *ApoE*$^{-/-}$ mice, which was confirmed by Western blot analysis (**D**). Immunofluorescence staining showed cytoplasmic and nuclear staining patterns of PPAR-γ in the MGs of WT mice, while only nuclear staining in the MGs of *ApoE*$^{-/-}$ mice (**E**). Western blot analysis showing decreased PPAR-γ expression in *ApoE*$^{-/-}$ mice (**F, G**). Data are shown as mean ± SD. $^{**}p < 0.01$. Scale bars: 50 μm.

ROSI, one time daily) + ROSI (10 mg/kg, oral gavage, one time daily) group (n = 10). Two months later, the mice were examined by slit-lamp microscopy before sacrifice. In the CON group, there was evidence of pannus formation in the cornea (Fig. 7A), whereas in the ROSI group, corneas remained transparent with a normal ocular surface throughout the observation period. In GW9662 + ROSI group, on the other hand, corneal pannus was also observed (Fig. 7A). Eyelids were excessively keratinized and hypertrophic in CON and GW9662 + ROSI groups (Fig. 7A), with no obvious abnormality in the ROSI group. Fluorescein staining scores, moreover, were significantly decreased after 2 months treatment with ROSI (Fig. 7B). Western blot analysis showed that PPAR-γ was increased after administration of ROSI, while p-NF-κB p65 was suppressed (Fig. 7C). Immuno-staining for PPAR-γ showed that ROSI increased the cytoplasmic expression of PPAR-γ in MG of *ApoE*$^{-/-}$ mice (Fig. 7D). IL-6, TNF-α, K10, and p-NF-κB p65 immuno-staining showed that ROSI application could decrease the expression of these inflammation and keratinization related proteins in the MG of *ApoE*$^{-/-}$ mice (Fig. 7D). CD45 staining also showed that ROSI could significantly decrease the inflammatory cell infiltration of MGs in *ApoE*$^{-/-}$ mice (Fig. 7E and F).

4. Discussion

Here, for the first time, we investigated the association between hyperlipidemia and MGD using an *ApoE*$^{-/-}$ mouse model for hyperlipidemia, which has been widely used for research into atherosclerosis and Alzheimer's disease. As previously reported [37], total cholesterol concentration in serum was dramatically increased in *ApoE*$^{-/-}$ mice compared with WT mice. Oil Red O staining showed accumulation of condensed lipids in the MGs of 5 and 7 month old *ApoE*$^{-/-}$ mice, indicating abnormal lipid metabolism in MGs.

We further characterized the clinical signs and pathological changes of MG in *ApoE*$^{-/-}$ mice, which showed consistent and definitive plugging of the MG orifice, in line with clinical observations supporting the idea that the plugging of the MG orifice is a pathognomonic sign of MGD [26,38]. Furthermore, *ApoE*$^{-/-}$ mice revealed cellular and

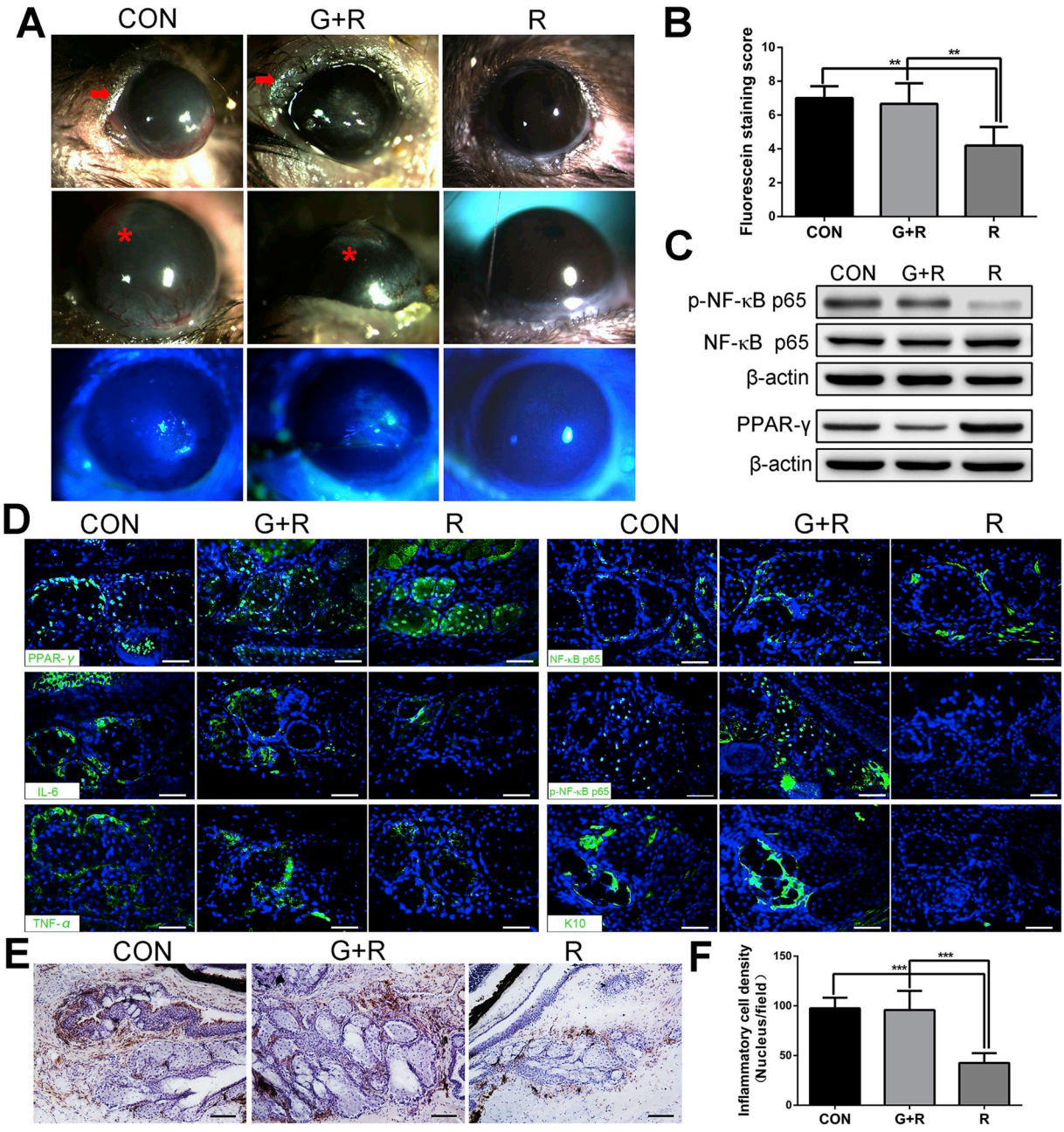

Fig. 7. PPAR-γ agonist treatment on *ApoE*$^{-/-}$ mice. Slit-lamp images indicating that ROSI treatment prevented pathological changes in the eyelid and cornea in *ApoE*$^{-/-}$ mice, with eyelid margin hypertrophy (arrow heads) and corneal neovascularization (asterisk) evident in the untreated *ApoE*$^{-/-}$ mice and GW9662 + ROSI treated *ApoE*$^{-/-}$ mice (**A**). The corneal fluorescein staining score decreased after ROSI treatment (**B**). Western blot analysis showing downregulated p-NF-κB p65 and upregulated PPAR-γ expression in the ROSI treatment group (**C**). Immunofluorescent staining showing decreased IL-6, TNF-α and K10 expression in the ROSI treatment group, along with an increased PPAR-γ expression (**D**). CD45 immunohistochemical staining showing decreased inflammatory cell infiltration in the ROSI treated group (**E**), confirmed by cell counting (**F**). Data are shown as mean ± SD. $^{**}p < 0.01$, $^{***}p < 0.001$. Scale bars: 50 μm. ROSI, Rosiglitazone; CON, control group; G + R, GW9662 + ROSI group; R, ROSI group.

morphological changes of the glands that are consistent with the histopathology of MGD. Such changes included the presence of eyelid hypertrophy, abnormal acini and dilated ducts [30,39–41]. We also observed MG dropout in *ApoE*$^{-/-}$ mice, which is congruent with results reported in patients with MGD [42]. K10 and FABP5 staining proved hyper-keratinization of MG duct and acinar cells; Ki67 and P63 staining supported decreased proliferation of acinar cells; TUNEL assay and AC-caspase-8 staining suggested elevated apoptosis of MG.

We found heightened ocular surface epithelial cell damage and corneal neovascularization in *ApoE*$^{-/-}$ mice at 5 and 7 months of age. Since we did not find significant lipid deposition in the cornea of *ApoE*$^{-/-}$ mice, the corneal neovascularization is not likely resulted from lipid keratopathy, which was reported to be one of the pathogenesis of corneal neovascularization [43]. Moreover, the ApoE gene expression is much lower in corneal and conjunctival tissue compared with that of MG (Figs. S1A and B), so the corneal pathological change may not directly induced by ApoE knockout. We proposed two underlying mechanisms of corneal neovascularization in *ApoE*$^{-/-}$ mice. Firstly, the inflammatory cytokines such as IL-6 and TNF-α were highly expressed in the MG of *ApoE*$^{-/-}$ mice, and the concentrations of these cytokines were also found increased in the aqueous tear of *ApoE*$^{-/-}$ mice (Figs. S2A and B). Such cytokines could induce neovascularization

in a long run of 5–7 months. Secondly, there was hyper-keratinization and thickening of the eyelid margin in *ApoE*$^{-/-}$ mice of 5–7 months old. Such eyelid margin changes may cause damage of the cornea during eyelid blinking and then result in neovascularization, which was reported in other eyelid margin related diseases [44,45].

Hyperkeratinization is a major reason for obstructive MGD and causes degenerative gland dilatation and atrophy [39]. Abnormal MG lipid is one of the factors that could induce epithelial keratinization and MG obstruction [35,46]. H&E staining showed dilation of MG ducts, while gene expression and immunofluorescence analyses demonstrated upregulated K10 and FABP5 expression in MG ducts and acinar cells of *ApoE*$^{-/-}$ mice. These results indicated that the MGs of 7-month-old *ApoE*$^{-/-}$ mice underwent hyperkeratosis which could lead to obstructive MGD, and progressive lipid accumulation in acini and ducts that likely triggers a vicious cycle of pathological change.

Inflammatory cell infiltration in the surrounding microenvironment of MGs in *ApoE*$^{-/-}$ mice may be attributed to hyperlipidemia and/or MGD. Hyperlipidemia can induce metabolic inflammation and the production of cytokines to damage vascular smooth muscle cells [47]. Hyperlipidemia can also induce infiltration of foamy macrophages in aortic adventitial, eventually leading to aortic dilation [48]. Reyes and associates have pointed to the important role for polymorphonuclear neutrophils in the pathogenesis and progression of MGD [49]. We found inflammatory cell infiltration of the eyelid by CD45 staining surrounding the microenvironment of the MGs, along with increased expression of inflammatory cytokines such as IL-6 and TNF-α in acinar cells. These changes mimic the histopathological, functional and inflammatory changes of MGD. NF-κB plays an important role in regulating innate immune and inflammatory responses [50,51]. Therefore, we investigated whether this finding is associated with an up-regulation of the NF-κB signaling pathway. The finding in the *ApoE*$^{-/-}$ mice that the NF-κB signaling pathway was activated in the MG of *ApoE*$^{-/-}$ mice further confirms the inflammatory environment of the MG.

Lipid oxidation may be another pathogenic mechanism inducing MG inflammation in *ApoE*$^{-/-}$ mice. Exaggerated lipid accumulation in acinar cells could, we hypothesized, have induced reactive oxygen species; this was confirmed by the expression of oxidation related markers in MGs. Oxidation is a well-known mechanism that promote inflammation in different tissues, and activates the expression of inflammatory cytokines [52,53]. PPAR-γ is the major signal controlling element for lipid synthesis and sebaceous gland function [54–56]. Oxidative stress can also modulate PPAR-γ expression [57]. We detected the down-regulation of PPAR-γ, along with an alteration in cytoplasmic and nuclear expression patterns of PPAR-γ to a solely nuclear pattern in MG of *ApoE*$^{-/-}$ mice. This is similar to age-related MGD [35]. Indeed, PPAR-γ dependent signaling is already known to play a role in inflammation control [58]. Therefore, down-regulation of PPAR-γ may be related to the inflammatory condition of the MGs in *ApoE*$^{-/-}$ mice. We then tested rosiglitazone, a PPAR-γ agonist, on the inflammation and keratinization of MGs in *ApoE*$^{-/-}$ mice, and found that the treatment significantly restored the expression pattern of PPAR-γ, consistent with previous reports [59]. Treatment also reduced expression of inflammatory cytokines IL-6 and TNF-α, downregulated NF-κB signaling pathway, reduced keratinization of MGs, and lowered inflammatory cell infiltration. Rosiglitazone also has potential anti-inflammatory effects on the ocular surface [60]. As a result, the effect of rosiglitazone on the MGs and ocular surface together prevented the ocular surface changes of *ApoE*$^{-/-}$ mice and resulted in a relatively healthy ocular surface being maintained. We therefore consider the PPAR-γ agonist to have a therapeutic effect on hyperlipidemia related MGD.

Based on our results, the inflammation of the MG acinar cells and the inflammation of surrounding microenvironment may both contribute to the pathogenesis of MGD in *ApoE*$^{-/-}$ mice. Which one plays the major role, or which one is the primary pathological process, or these two processes form a vicious cycle need further investigation. In summary, *ApoE*$^{-/-}$ mice showed MG obstruction with MG dropout, excessive keratinization, abnormal MG acinar cell proliferation, differentiation, lipid metabolism and an increased inflammatory cell infiltration in the MG, thus leading to obstructive MGD and ocular surface changes. *ApoE*$^{-/-}$ mice may be used as a model to study the pathophysiology of MGD and may help us to understand the relationship between lipid metabolism related disorders and MGD.

Conflicts of interest

The authors have declared no competing interest and financial or business interest related to this study.

Acknowledgments

This study was supported in part by the National Key R&D Program of China (2018YFA0107301, 2018YFA0107304), the National Natural Science Foundation of China (NSFC, No.81770894, No.81470602 and No.81330022). The funders had no role in study design, data collection and analysis, decision on publish, or preparation of the manuscript.

Appendix A. Supplementary data

Supplementary data to this article can be found online at https://doi.org/10.1016/j.jtos.2019.06.002.

References

[1] Jester JV, Nicolaides N, Smith RE. Meibomian gland studies: histologic and ultrastructural investigations. Investig Ophthalmol Vis Sci 1981;20:537–47.
[2] Bron AJ, Benjamin L, Snibson GR. Meibomian gland disease. Classification and grading of lid changes. Eye 1991;5(Pt 4):395–411.
[3] Willcox MDP, Argueso P, Georgiev GA, Holopainen JM, Laurie GW, Millar TJ, et al. TFOS DEWS II tear film report. Ocul Surf 2017;15:366–403.
[4] Holly FJ, Lemp MA. Tear physiology and dry eyes. Surv Ophthalmol 1977;22:69–87.
[5] Wang YC, Li S, Chen X, Ma B, He H, Liu T, et al. Meibomian gland absence related dry eye in ectodysplasin a mutant mice. Am J Pathol 2016;186:32–42.
[6] Butovich IA. Meibomian glands, meibum, and meibogenesis. Exp Eye Res 2017;163:2–16.
[7] Nelson JD, Shimazaki J, Benitez-del-Castillo JM, Craig JP, McCulley JP, Den S, et al. The international workshop on meibomian gland dysfunction: report of the definition and classification subcommittee. Investig Ophthalmol Vis Sci 2011;52:1930–7.
[8] Bron AJ, Tiffany JM. The contribution of meibomian disease to dry eye. Ocul Surf 2004;2:149–65.
[9] Schaumberg DA, Nichols JJ, Papas EB, Tong L, Uchino M, Nichols KK. The international workshop on meibomian gland dysfunction: report of the subcommittee on the epidemiology of, and associated risk factors for, MGD. Investig Ophthalmol Vis Sci 2011;52:1994–2005.
[10] Miljanovic B, Dana R, Sullivan DA, Schaumberg DA. Impact of dry eye syndrome on vision-related quality of life. Am J Ophthalmol 2007;143:409–15.
[11] Denoyer A, Rabut G, Baudouin C. Tear film aberration dynamics and vision-related quality of life in patients with dry eye disease. Ophthalmology 2012;119:1811–8.
[12] Blue ML, Williams DL, Zucker S, Khan SA, Blum CB. Apolipoprotein E synthesis in human kidney, adrenal gland, and liver. Proc Natl Acad Sci USA 1983;80:283–7.
[13] Breslow JL, Zannis VI, SanGiacomo TR, Third JL, Tracy T, Glueck CJ. Studies of familial type III hyperlipoproteinemia using as a genetic marker the apoE phenotype E2/2. JLR (J Lipid Res) 1982;23:1224–35.
[14] Zhang HL, Wu J, Zhu J. The role of apolipoprotein E in Guillain-Barre syndrome and experimental autoimmune neuritis. J Biomed Biotechnol 2010;2010:357412.
[15] Meir KS, Leitersdorf E. Atherosclerosis in the apolipoprotein-E-deficient mouse: a decade of progress. Arterioscler Thromb Vasc Biol 2004;24:1006–14.
[16] Buzello M, Tornig J, Faulhaber J, Ehmke H, Ritz E, Amann K. The apolipoprotein e knockout mouse: a model documenting accelerated atherogenesis in uremia. J Am Soc Nephrol : JASN (J Am Soc Nephrol) 2003;14:311–6.
[17] Subbiah MT, Deitemeyer D, Yunker R. Regional aortic differences in atherosclerosis susceptibility. Relationship to lipid concentration and prostaglandin biosynthesis. Virchows Arch B Cell Pathol Incl Mol Pathol 1981;36:41–6.
[18] Smith JD, Breslow JL. The emergence of mouse models of atherosclerosis and their relevance to clinical research. J Intern Med 1997;242:99–109.
[19] Osada J, Joven J, Maeda N. The value of apolipoprotein E knockout mice for studying the effects of dietary fat and cholesterol on atherogenesis. Curr Opin Lipidol 2000;11:25–9.
[20] Braich PS, Howard MK, Singh JS. Dyslipidemia and its association with meibomian gland dysfunction. Int Ophthalmol 2016;36:469–76.
[21] Dao AH, Spindle JD, Harp BA, Jacob A, Chuang AZ, Yee RW. Association of

dyslipidemia in moderate to severe meibomian gland dysfunction. Am J Ophthalmol 2010;150:371–5. e1.
[22] Bukhari AA. Associations between the grade of meibomian gland dysfunction and dyslipidemia. Ophthalmic Plast Reconstr Surg 2013;29:101–3.
[23] Lin Z, Liu X, Zhou T, Wang Y, Bai L, He H, et al. A mouse dry eye model induced by topical administration of benzalkonium chloride. Mol Vis 2011;17:257–64.
[24] Zadelaar S, Kleemann R, Verschuren L, de Vries-Van der Weij J, van der Hoorn J, Princen HM, et al. Mouse models for atherosclerosis and pharmaceutical modifiers. Arterioscler Thromb Vasc Biol 2007;27:1706–21.
[25] Yin Y, Gong L. Reversibility of gland dropout and significance of eyelid hygiene treatment in meibomian gland dysfunction. Cornea 2017;36:332–7.
[26] Foulks GN, Bron AJ. Meibomian gland dysfunction: a clinical scheme for description, diagnosis, classification, and grading. Ocul Surf 2003;1:107–26.
[27] Senoo M, Pinto F, Crum CP, McKeon F. p63 Is essential for the proliferative potential of stem cells in stratified epithelia. Cell 2007;129:523–36.
[28] Jester JV, Rife L, Nii D, Luttrull JK, Wilson L, Smith RE. In vivo biomicroscopy and photography of meibomian glands in a rabbit model of meibomian gland dysfunction. Investig Ophthalmol Vis Sci 1982;22:660–7.
[29] Jester JV, Rajagopalan S, Rodrigues M. Meibomian gland changes in the rhino (hrrhhrrh) mouse. Investig Ophthalmol Vis Sci 1988;29:1190–4.
[30] Knop E, Knop N, Millar T, Obata H, Sullivan DA. The international workshop on meibomian gland dysfunction: report of the subcommittee on anatomy, physiology, and pathophysiology of the meibomian gland. Investig Ophthalmol Vis Sci 2011;52:1938–78.
[31] Ouellet T, Lussier M, Babai F, Lapointe L, Royal A. Differential expression of the epidermal K1 and K10 keratin genes during mouse embryo development. Biochem Cell Biol = Biochim Biol Cell 1990;68:448–53.
[32] Dallaglio K, Marconi A, Truzzi F, Lotti R, Palazzo E, Petrachi T, et al. E-FABP induces differentiation in normal human keratinocytes and modulates the differentiation process in psoriatic keratinocytes in vitro. Exp Dermatol 2013;22:255–61.
[33] Ogawa E, Owada Y, Ikawa S, Adachi Y, Egawa T, Nemoto K, et al. Epidermal FABP (FABP5) regulates keratinocyte differentiation by 13(S)-HODE-mediated activation of the NF-kappaB signaling pathway. J Investig Dermatol 2011;131:604–12.
[34] Trivedi NR, Cong Z, Nelson AM, Albert AJ, Rosamilia LL, Sivarajah S, et al. Peroxisome proliferator-activated receptors increase human sebum production. J Investig Dermatol 2006;126:2002–9.
[35] Nien CJ, Paugh JR, Massei S, Wahlert AJ, Kao WW, Jester JV. Age-related changes in the meibomian gland. Exp Eye Res 2009;89:1021–7.
[36] Nien CJ, Massei S, Lin G, Nabavi C, Tao J, Brown DJ, et al. Effects of age and dysfunction on human meibomian glands. Arch Ophthalmol 2011;129:462–9.
[37] Hinder LM, Vincent AM, Hayes JM, McLean LL, Feldman EL. Apolipoprotein E knockout as the basis for mouse models of dyslipidemia-induced neuropathy. Exp Neurol 2013;239:102–10.
[38] McCulley JP, Dougherty JM, Deneau DG. Classification of chronic blepharitis. Ophthalmology 1982;89:1173–80.
[39] Jester JV, Nicolaides N, Kiss-Palvolgyi I, Smith RE. Meibomian gland dysfunction. II. The role of keratinization in a rabbit model of MGD. Investig Ophthalmol Vis Sci 1989;30:936–45.
[40] Parfitt GJ, Xie Y, Geyfman M, Brown DJ, Jester JV. Absence of ductal hyper-keratinization in mouse age-related meibomian gland dysfunction (ARMGD). Aging 2013;5:825–34.
[41] Obata H. Anatomy and histopathology of human meibomian gland. Cornea 2002;21:S70–4.
[42] Arita R, Itoh K, Inoue K, Amano S. Noncontact infrared meibography to document age-related changes of the meibomian glands in a normal population. Ophthalmology 2008;115:911–5.
[43] Crispin S. Ocular lipid deposition and hyperlipoproteinaemia. Prog Retin Eye Res 2002;21:169–224.
[44] Suzuki T. Inflamed obstructive meibomian gland dysfunction causes ocular surface inflammation. Investig Ophthalmol Vis Sci 2018;59:Des94–101.
[45] Bergstrom R, Czyz CN. Entropion. StatPearls. Treasure island (FL). StatPearls Publishing StatPearls Publishing LLC.; 2019.
[46] Hykin PG, Bron AJ. Age-related morphological changes in lid margin and meibomian gland anatomy. Cornea 1992;11:334–42.
[47] Clarke MC, Talib S, Figg NL, Bennett MR. Vascular smooth muscle cell apoptosis induces interleukin-1-directed inflammation: effects of hyperlipidemia-mediated inhibition of phagocytosis. Circ Res 2010;106:363–72.
[48] Freestone T, Turner RJ, Higman DJ, Lever MJ, Powell JT. Influence of hypercholesterolemia and adventitial inflammation on the development of aortic aneurysm in rabbits. Arterioscler Thromb Vasc Biol 1997;17:10–7.
[49] Reyes NJ, Yu C. Neutrophils cause obstruction of eyelid sebaceous glands in inflammatory eye disease in mice vol. 10. 2018.
[50] Li Q, Verma IM. NF-kappaB regulation in the immune system. Nat Rev Immunol 2002;2:725–34.
[51] Baker RG, Hayden MS, Ghosh S. NF-kappaB, inflammation, and metabolic disease. Cell Metabol 2011;13:11–22.
[52] Satapati S, Kucejova B, Duarte JA, Fletcher JA, Reynolds L, Sunny NE, et al. Mitochondrial metabolism mediates oxidative stress and inflammation in fatty liver. J Clin Investig 2015;125:4447–62.
[53] Gill R, Tsung A, Billiar T. Linking oxidative stress to inflammation: toll-like receptors. Free Radical Biol Med 2010;48:1121–32.
[54] Imai T, Takakuwa R, Marchand S, Dentz E, Bornert JM, Messaddeq N, et al. Peroxisome proliferator-activated receptor gamma is required in mature white and brown adipocytes for their survival in the mouse. Proc Natl Acad Sci USA 2004;101:4543–7.
[55] Nien CJ, Massei S, Lin G, Liu H, Paugh JR, Liu CY, et al. The development of meibomian glands in mice. Mol Vis 2010;16:1132–40.
[56] Gervois P, Fruchart JC, Staels B. Inflammation, dyslipidaemia, diabetes and PPars: pharmacological interest of dual PPARalpha and PPARgamma agonists. Int J Clin Pract Suppl 2004:22–9.
[57] Sommer M, Wolf G. Rosiglitazone increases PPARgamma in renal tubular epithelial cells and protects against damage by hydrogen peroxide. Am J Nephrol 2007;27:425–34.
[58] Delerive P, Fruchart JC, Staels B. Peroxisome proliferator-activated receptors in inflammation control. J Endocrinol 2001;169:453–9.
[59] Jester JV, Potma E, Brown DJ. PPARgamma regulates mouse meibocyte differentiation and lipid synthesis. Ocul Surf 2016;14:484–94.
[60] Huxlin KR, Hindman HB, Jeon KI, Buhren J, MacRae S, DeMagistris M, et al. Topical rosiglitazone is an effective anti-scarring agent in the cornea. PLoS One 2013;8:e70785.